Submitted: August 12, 2025 Revised: September 8, 2025 Accepted: October 7, 2025

Fabrication and characterization of NiO/AZO heterojunction thin film diodes by radio frequency magnetron sputtering

B.Q. Tran* [1], T.N.H. Ngo* [1], K.B. Nguyen[2,3], H.D.T. Duong [1], B.K. Thach [1], H.P. Pham [2,3], H.D. Ngo [1], T.K.H. Pham [1]✉

[1] Ho Chi Minh City University of Technology and Education, Ho Chi Minh City, Vietnam

[2] Nguyen Tat Thanh University Center for Hi-Tech Development, Saigon Hi-Tech Park, Ho Chi Minh City, Vietnam

[3] NTT Hi-Tech Institute, Nguyen Tat Thanh University, Ho Chi Minh City, Vietnam

✉ hangptk@hcmute.edu.vn

*These authors contributed equally to this work.

ABSTRACT

This study focuses on the fabrication and investigation of the properties of the heterojunction *p*-NiO/*n*-Al-doped ZnO via the radio frequency magnetron sputtering method. We conducted a detailed evaluation of the crystal structure, optical properties, and electrical properties of the NiO and Al-doped ZnO monolayers using advanced techniques such as X-ray diffraction, ultraviolet-visible spectroscopy, and Hall effect measurements. X-ray diffraction results show that the NiO thin film crystallizes in the (111) and (200) peaks with a characteristic NaCl-type cubic structure, while the Al-doped ZnO thin film preferentially develops in the (002) peak, exhibiting a hexagonal wurtzite structure. UV–Vis transmission spectrum analysis indicates that the NiO and Al-doped ZnO thin films exhibit transmittance rates of 52 and 92 % in the visible light region, respectively. The optical band gap energy was determined to be 3.45 eV for NiO and 3.36 eV for Al-doped ZnO, respectively. In addition, the carrier concentration in both single layers reached a high level, around 10^{19} cm^{-3}. The *J-V* characteristics under optimal conditions confirmed the formation of the NiO/AZO heterojunction with a turn-on voltage of 0.67 V, an ideality factor of 4.44, and a barrier potential height of 0.5 eV. Especially, the influence of light with a wavelength of 365 nm, this heterojunction clearly exhibited the characteristics of a photodiode. These results demonstrate the remarkable potential applications of the *p*-NiO/*n*-AZO heterojunction in the fields of optoelectronics and light sensors.

KEYWORDS

Al-doped ZnO • NiO • photodiode • heterojunction • RF-magnetron sputtering

Funding. *This work has been supported by the grant of the Ho Chi Minh city university of Technology and Education (SV2025–30).*

Citation: Tran BQ, Ngo TNH, Nguyen KB, Duong HDT, Thach BK, Pham HP, Ngo HD, Pham TKH. Fabrication and characterization of NiO/AZO heterojunction thin film diodes by radio frequency magnetron sputtering. *Materials Physics and Mechanics.* 2025;53(3): 120–130.
http://dx.doi.org/10.18149/MPM.5312025_10

Introduction

UV photodiodes based on semiconductor materials with a large bandgap energy (E_g > 3 eV) are becoming a focal research area due to their widespread applications in the ultraviolet region [1]. Typical materials in the class of transparent conducting oxides (TCOs) include TiO_2, ZnO, NiO, SnO_2, and Ga_2O_3. Among these, ZnO and NiO stand out with their unique optoelectronic properties. They not only have an impressive transmittance (up to 80 %) in the visible region but also possess a low resistivity, around 10^{-3} Ω·cm at room temperature [2–4]. Moreover, their abundant availability, low cost, and environmental friendliness make them highly attractive for potential large-scale industrial applications. In practice, however, the fabrication of photodiodes based on ZnO/NiO heterojunctions faces significant challenges, particularly in achieving stable *p*-type ZnO (doped with N, P, As, or Sb) and *n*-type NiO (doped with Al, Li, Ag, or Cu). These difficulties arise from the low solubility of dopants, the self-compensation effect, and the limited ability to maintain the desired conductivity type [5–7]. Consequently, heterojunctions employing ZnO or NiO are being actively investigated for optoelectronic applications [8–10].

Zinc oxide (ZnO) is an *n*-type semiconductor belonging to the II-VI group, exhibiting a hexagonal wurtzite structure with space group $P6_3mc$ and lattice constants a = 3.25 Å and c = 5.20 Å [1]. Moreover, its direct bandgap energy of approximately 3.37 eV and a large exciton energy of 60 meV make ZnO highly suitable for a wide range of applications, including UV sensors, UV photoconductive detectors, and white light-emitting devices [11–16]. The *n*-type semiconductor properties of ZnO are primarily formed by intrinsic defects such as zinc interstitial and oxygen vacancy. However, increasing the defect density in the ZnO crystal lattice to enhance its electrical properties inevitably deteriorates both its crystalline quality and optical characteristics. Therefore, to preserve the structural integrity and optoelectronic performance, the carrier concentration of intrinsic ZnO is typically maintained in the range of 10^{16} – 10^{17} cm^{-3} [17]. This procedure causes high resistivity, significantly limiting the performance of the device. To overcome these problems, group IIIA metals like Al, Ga, and In are often added to the ZnO crystal lattice to increase the number of carriers while keeping the crystal's high transparency in the visible range [18–20]. Al is the most common dopant because it works well to replace Zn atoms and is cheaper than In and Ga [21]. Furthermore, high-quality Al-doped ZnO (AZO) thin films can be readily fabricated using various techniques, including radio frequency (RF) magnetron sputtering, metal–organic chemical vapor deposition, and atomic layer deposition.

Nickel oxide (NiO) is a highly promising material for forming *p*–*n* junctions with ZnO. It crystallizes in a face-centered cubic rock-salt structure (space group *Fm-3m*) with a lattice constant of a ~ 4.17 Å [1]. Owing to its oxygen sublattice having a hexagonal symmetry similar to that of Al-doped ZnO, NiO can be effectively deposited on this substrate [22]. As an intrinsic *p*-type semiconductor with a wide direct bandgap of 3.4–4.0 eV, NiO is an attractive candidate for UV sensor applications [23]. Its hole conductivity arises primarily from nickel vacancies and oxygen interstitials; however, its carrier concentration is generally limited. In our previous work, RF-reactive magnetron sputtering was employed to self-dope NiO by controlling the reactive gas flow and the Ni^{3+} content, which serves as a source of free carriers. This approach enabled the carrier concentration to exceed 10^{19} cm^{-3} [24].

Up to now, research on the fabrication and application of NiO/AZO-based heterojunctions remains limited. Shu-Yi Tsai *et al.* fabricated NiO/ZnO heterojunctions via RF magnetron sputtering, reporting carrier concentrations of 7.52×10^{18} and 4.29×10^{19} cm^{-3}, mobilities of 2.26 and 6.02 $cm^2/V{\cdot}s$, and ~ 80 % transmittance in the visible range for single-layer NiO and ZnO, respectively. The resulting heterojunction exhibited an open-circuit voltage of ~2.5 eV and UV sensitivity at 365 nm [25]. Similarly, Gupta R.K. et al. produced *p*-NiO/*n*-ZnO heterojunctions by pulsed laser deposition, achieving transmittances of 64 and 87 %, carrier concentrations of 7.1 × 10^{18} and 6.5 × 10^{19} cm^{-3}, and an open-circuit voltage of 0.45 eV with an ideality factor of about 4.1 and a barrier potential of about 0.35 eV (determined by Norde's method) [26]. However, the large carrier concentration mismatch between NiO and ZnO resulted in a non-optimal electric field distribution in the depletion region, limiting photo-generated carrier collection. NiO/ZnO heterojunctions have been investigated for applications such as photocatalysis, formaldehyde and trimethylamine sensing, UV photodetectors, and supercapacitors [27–31].

In this work, we fabricated a *p*–*n* NiO/AZO heterojunction via RF magnetron sputtering–a widely adopted method offering good uniformity, deposition rate, adhesion, and industrial scalability [32]. Film thickness and properties can be precisely tuned by controlling oxygen flow rate, sputtering power, substrate temperature, and annealing temperature, as demonstrated in our previous studies. Here, we successfully prepared the heterojunction for ultraviolet light sensing applications. While the crystal structure, optical, and electrical properties of the AZO and NiO single layers have been reported previously, this study focuses on investigating the carrier transport mechanism under dark and UV-illuminated (365 nm) conditions through *J*–*V* characterization, which points to possibilities for the potential for practical device applications. XRD, UV–Vis, and Hall effect results are taken from our earlier publications [33, 34].

Materials and Methods

The AZO thin film was fabricated on a glass substrate using the radio frequency (RF) magnetron sputtering, with Al-doped ZnO lab-made targets (2 at. % Al). The glass substrate was thoroughly cleaned with acetone, ethanol, and isopropyl alcohol (IPA), each solution for 5 mins, and then heated in a vacuum chamber at a pressure of 5 × 10^{-3} Torr to completely remove impurities and moisture. The AZO film deposition process was carried out at a temperature of 200 °C and a power of 50 W. Next, NiO thin films were sputtered onto the prepared AZO/glass structure, using a Ni metal target with a purity of 99.95% in an argon and oxygen gas environment (Fig. 1). The optimal deposition conditions were established at a pressure of 5 × 10^{-3} Torr, an RF power of 70 W, and an Ar:O_2 gas ratio of 7:3. The substrate temperature is maintained at a stable 250 °C throughout the sputtering process. Indium was used as the electrode material. The contacts were deposited by sputtering through a shadow mask, which allowed indium to contact both the NiO and AZO layers (Fig. 1). The NiO thin film exhibited a thickness of approximately 250 nm, while the AZO thin film showed a thickness of about 280 nm. The crystal structure of the films was analyzed using X-ray diffraction (XRD, D8-ADVANCE).

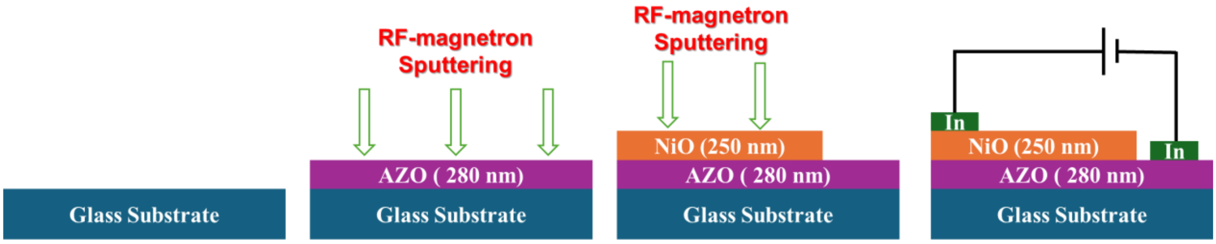

Fig 1. The process of fabricating a *p*-NiO/*n*-AZO heterojunction using the RF-magnetron sputtering method

The optical properties were evaluated through UV-Vis (JASCO, V-550, Japan) transmission spectra, while the electrical characteristics were investigated in detail using Hall effect measurements (BIO-RAD HL5500IU). Finally, the $I-V$ characteristics of the diode were measured at room temperature using a Keysight-U2722A current-voltage source.

Results and Discussion

The structural characteristics of AZO and NiO thin films fabricated using the RF-magnetron sputtering method were previously reported in references [33] and [34]. The AZO thin film exhibits a high-intensity difraction peak (002) at an angle of 2θ= 34.54°, with a full width at half maximum (FWHM) of approximately 0.25°. This observation confirms that the AZO thin film crystallizes in the characteristic hexagonal wurtzite structure, with the c lattice constant (denoted as a_2) determined to be 5.19 Å [33]. Meanwhile, the diffraction pattern of NiO thin film shows the appearance of two main peaks: (111) at 2θ = 36.43° and (200) at 2θ = 42.73° with corresponding FWHM values of 2.13° and 1.07°, respectively. These peaks represent the characteristic of the cubic structure of NiO, with the lattice constant a (denoted as a_1) estimated to be approximately 4.25 Å [34]. Although the crystal structures of AZO thin films (hexagonal wurtzite) and NiO (NaCl-type cubic) are different, the deposition of high-quality ZnO layers on NiO substrates is still feasible because of the similar oxygen atom configuration (six-fold symmetry) [22].

To further confirm the electrical characterization results and support energy band alignment, an analysis of the lattice mismatch at the NiO/ZnO interface was conducted. The estimation was performed using equations commonly applied to materials with cubic crystal structures [35]. Based on this assumption, the lattice mismatch values were calculated using the following expression:

$$\Delta a = \frac{2(a_1 - a_2)}{a_1 + a_2}, \quad (1)$$

$$N_s = \frac{4(a_1^2 + a_2^2)}{a_1^2 a_2^2}, \quad (2)$$

$$x = \frac{a_1 a_2}{\sqrt{2}\,(a_1 + a_2)}, \quad (3)$$

where a_1, a_2 represents the lattice parameters of the contacting material, N_s is the minimum concentration of surface states at the heterojunction, x is the average distance between NiO and AZO thin films.

Table 1. Lattice mismatch and interfacial parameters of AZO and NiO thin films at the heterojunction

Sample	2θ, °	(hkl)	Lactice parameter		Δa, %	x, 10^7 cm	N_s, 10^{-13} cm^{-2}
			a_1, Å	a_2, Å			
AZO	34.54	(002)	–	5.19	-19.92	1.65	3.7
Nio	36.43	(111)	4.25	–			
	42.73	(200)					

The lattice constant deviation between NiO (cubic) and AZO (hexagonal) was calculated to be −19.92%, indicating a significant mismatch at the NiO/AZO heterojunction. In comparison, an ideal heterojunction typically exhibits a lattice mismatch below 7 % [35]. The significant mismatch leads to the formation of interfacial defects, with an estimated surface state density of 3.7×10^{-13} cm^{-2}. These defects facilitate the recombination of charge carriers during the charge transport process. The lattice parameters, mismatch values, and interfacial characteristics of the NiO and AZO thin films, as well as their heterojunction, are summarized in Table 1.

In our previous report [33,34], the optical properties of NiO and AZO thin films were analyzed by using the UV-Vis spectroscopy in the wavelength range from 300 to 1000 nm. The average transmittance was determined to be 92 and 52 % in the visible light region, respectively. Based on the results of the transmission spectrum, the absorption coefficient was determined in the strong absorption region according to the Beer-Lambert law [36]:

$$\alpha = d^{-1}\left[\ln\left(\frac{1}{T}\right)\right], \tag{4}$$

where T is the normalized transmittance and d is the thickness of the film (280 nm for AZO and 250 nm for NiO). The optical band gap (E_g) was then determined using Tauc's formula [36]:

$$\alpha h v = A\left(h v - E_g\right)^k, \tag{5}$$

where α is the absorption coefficient, A is the band edge constant, hv is the photon energy, and k = 1/2 for direct allowed transition, as in the hexangonal wurtzite structure of AZO and the cubic structure of NiO. The optical band gap energy is determined to be 3.36 eV for the AZO thin film and 3.45 eV for the NiO thin film.

Moreover, the electrical properties of AZO and NiO thin films were determined by Hall effect measurements [33,34]. Based on the values indicating the carrier concentration, the NiO and AZO films exhibit *p*-type and *n*-type semiconductor properties, respectively. The carrier concentration and mobility for the AZO thin film were determined to be 2.19×10^{19} cm^{-3} and 0.9 cm^2/V·s, respectively, while for the NiO thin film, they were 2.36×10^{19} cm^{-3} and 1.02 cm^2/V·s, respectively. The parameters characterizing the optical and electrical properties of the AZO and NiO single-layer films are summarized in Table 2.

Table 2. Optical and electrical properties of AZO and NiO thin films

Sample	Thickness, nm	*T* %, 400–800 nm	Optical bandgap, eV	Carrier type	Carrier concentration, 10^{19} cm^{-3}	Mobility, cm^2/V·s	Ref.
AZO	280	92	3.36	*n*	-2.19	0.9	[33]
NiO	250	52	3.45	*p*	+2.36	1.02	[34]

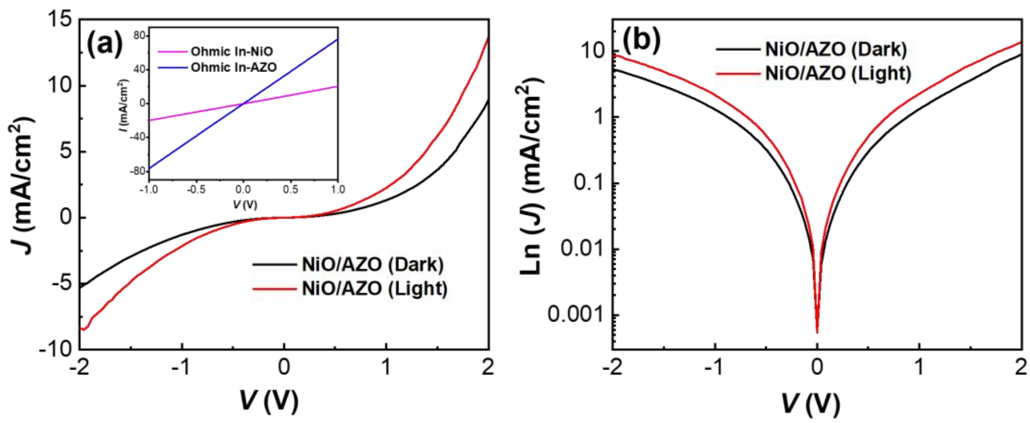

Fig 2. Linear (a) and semi-logarithmic (b) *J–V* characteristics of the NiO/AZO diode

Indium metal was used for ohmic contact with the AZO and NiO thin films with a work function of 4.12 eV, as shown in the inset Fig. 2(a). The results show that the p-type semiconductor NiO has formed a heterojunction on the *n*-type AZO semiconductor substrate with the NiO/AZO/glass diode structure. The *J–V* characteristics in the dark mode and the changes in characteristics under illumination are shown in Fig. 2(a) (linear) and Fig. 2(b) (semi-logarithmic), with the open-circuit voltage V_{oc} (dark) determined to be 0.67 V, consistent with previous reports [37]. In addition, the relatively large leakage current due to the sputtering fabrication method causes the surface of the AZO film to suffer damage from ion bombardment before the NiO thin film is deposited [3].

The *J–V* characteristic curve represents the rectifying relationship between the current density through the diode and the voltage according to the thermionic emission theory given by the expression [24,38]:

$$J = J_0 \cdot \exp\left(\frac{qV}{nK_BT} - 1\right). \quad (6)$$

Here q is the electron charge (1.6×10^{-19} C), K_B is Boltzmann constant ($J \cdot K^{-1}$), T is the absolute temperature (K) and J_0 is the reverse saturation current:

$$J_0 = AA^*T^2 \exp\left(\frac{-q\phi_B}{K_BT}\right), \quad (7)$$

where A is the area of the diode (1 cm^2); A^* is the Richardson constant of the *p*-NiO/*n*-ZnO heterojunction (0.062 A $cm^{-2} \cdot K^{-2}$) [39].

The effective barrier height is determined [24,38]:

$$\phi_B = \frac{K_BT}{q} ln \frac{AA^*T^2}{J_0}, \quad (8)$$

with J_0 determined from the extrapolated results in the linear region of the ln(J) curve with respect to V at the time $V = 0$.

ln(J) is determined:

$$\ln J = \frac{qV}{nK_BT} + \ln J_o. \quad (9)$$

The ideal factor (n) is determined:

$$n = \frac{q}{K_BT} \cdot \frac{dV}{dlnJ}. \quad (10)$$

Under dark light, the ideality factor (n) and effective barrier height (ϕ_B) are determined to be 4.44 and 0.50 eV, respectively. The diode operates based on two main mechanisms: thermal transport (TE) and the tunneling effect [40]. The TE mechanism for an ideal diode is the movement of charge carriers due to temperature. Conversely, tunneling allows charge carriers to pass through the energy barrier, often dominating when the diode has a low ideality factor or a large energy barrier. According to the Sah-Noyce-Shockley theory, the ideality factor ranges from 1 to 2, indicating that the primary current mechanism is due to the tunneling effect [40]. If $n = 2$, the dominant mechanism is due to recombination and emission; if $n > 2$, the dominant mechanism is leakage current [40]. The high ideality factor value of the NiO/AZO diode is explained by the following reasons: (i) the high series resistance of the two material layers; (ii) the recombination of charge carriers in the depletion region; (iii) the surface morphology of the material; (iv) charge carriers tunneling between states in the bandgap; and (v) inhomogeneous potential barrier [41]. Furthermore, Table 3 shows that the *p*-NiO/*n*-AZO diode fabricated in this study exhibits a threshold voltage significantly lower than that reported in many previous studies on NiO/ZnO systems (1.0 – 3.0 V). This suggests that the use of Al-doped ZnO, combined with a balanced carrier concentration between the two junction layers, contributes to lowering the threshold voltage, thereby reducing energy consumption and facilitating integration into low-voltage circuits.

Table 3. Comparison of turn-on voltage (V_{on}) and ideality factor (n) for NiO/AZO heterojunction diodes

Heterojunction structure	Method	V_{on}, V	Ideality factor	Ref.
In/NiO/AZO/In	Sputtering	0.67	4.44	This work
Au/NiO/ZnO/Au	PLD	~ 0.35	4.10	[26]
Al/NiO/ZnO/Al	Sputtering	~ 3.00	–	[25]
Au/ZnO/NiO:Li/ITO	PLD	1.00	2.00	[22]
Pt/NiO/ZnO/ITO	Sputtering	0.5−1.1	1.36−1.41	[42]
C/ZnO/NiO_x/Au	Inkjet printing	2.20	–	[43]
Au/NiO/ZnO/Au	Sputtering	1.3	2.7	[44]

Under the condition of illumination with a monochromatic light source at a wavelength of 365 nm (in the near-ultraviolet region), with a power of 10 W, the NiO/AZO heterojunction diode shows a significant increase in current in both polarities, especially in the reverse bias region. Illumination generates electron-hole pairs (e^-−h^+) in the *p-n* junction region, thereby increasing the carrier density and significantly contributing to the photocurrent. Under these conditions, the reverse current (photocurrent) increases significantly, reflecting the structure's ability to efficiently absorb photons and effectively separate charge carriers. This shows that the diode operates effectively as an ultraviolet photodiode, with high sensitivity in the light region where the photon energy is greater than the bandgap of the absorbing material. The analysis results show its potential application in optoelectronic devices such as photodiodes or solar cells.

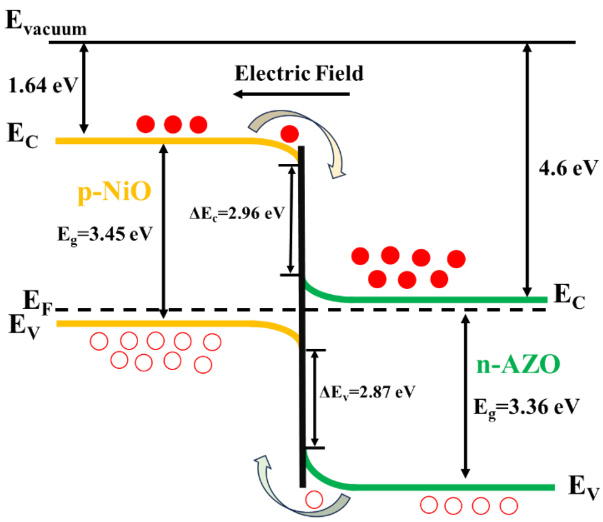

Fig 3. Band diagram of heterojuntion *p*-NiO/*n*-AZO

The energy band structure of the NiO/AZO heterostructure is illustrated in Fig. 3. The work function of the indium electrode is 4.12 eV. The electron affinities (χ) of NiO and AZO are 1.64 eV and 4.60 eV, respectively; the corresponding bandgap energies are 3.45 eV (NiO) and 3.36 eV (AZO) [45,46]. When two materials come into contact to form a heterostructure, the rearrangement of energy levels leads to the formation of potential barriers at the interface. The conduction band offset (ΔE_C) and valence band offset (ΔE_V) are determined according to equations [35]:

$$\Delta E_C = E_{C1} - E_{C2} = \chi_2 - \chi_1, \quad (11)$$

$$\Delta E_V = E_{V1} - E_{V2} = (\chi_1 + E_{g1}) - (\chi_2 + E_{g2}). \quad (12)$$

The conduction band and valence band offsets were determined to be 2.96 eV and 2.87 eV, respectively, based on the Anderson model, consistent with previous reports [37,47]. These two quantities indicate that the NiO/AZO heterojunction belongs to type II (type-II band alignment), where both the conduction band and valence band of AZO are lower than those of NiO. These two quantities indicate that the NiO/AZO heterojunction belongs to type II, where both the conduction band and the valence band of AZO are lower than those of NiO [48]. The distribution of energy bands in this manner facilitates the separation of electron-hole pairs (e^-−h^+). Specifically, electrons in the conduction band of NiO will easily move to the conduction band of AZO with a lower energy level, while holes in the valence band of AZO will move to the valence band of NiO. This process helps prevent recombination, thereby increasing the efficiency of charge separation generated under illumination, contributing to the enhancement of the performance of optoelectronic devices.

Conclusions

The photodiode on a *p*-NiO/*n*-AZO/glass substrate was fabricated using the RF-magnetron sputtering method. The NiO film, which has a cubic structure and a thickness of approximately 250 nm, is deposited on the AZO film, which has a hexagonal wurtzite structure and a thickness of approximately 280 nm. The optoelectronic properties of the single-layer films were determined using UV-Vis and Hall effect, with the NiO thin film (T % = 52 %, E_g = 3.45 eV, n_h = 2.36 × 10^{19} cm^{-3}, μ_h = 1.02 cm^2/V·s) and the AZO thin film (T % =92 %, E_g = 3.36 eV, n_h = 2.19 × 10^{19} cm^{-3}, μ_h = 0.90 cm^2/V·s). The *J*–*V* characteristics in dark and under illumination with a wavelength of 365 nm show that a heterojunction *p-n* is formed with diode-like properties in the dark, such as turn-on voltage, ideality factor, and barrier potential, which are determined to be 0.67 V, 4.44 and 0.5 eV, respectively, and also demonstrate good photodetection capability under ultraviolet light (356 nm). The results indicate that the NiO/AZO transition has potential applications in photodetectors in the future.

CRediT authorship contribution statement

Bao Quan Tran: writing – review & editing, writing – original draft; **Thi Nhu Huynh Ngo:** writing – review & editing, writing – original draft; **Khac Binh Nguyen:** investigation; **Hong Diu Tho Duong:** investigation; **Bao Khang Thach:** investigation; **Hoai Phuong Pham:** data curation, conceptualization; **Hai Dang Ngo:** data curation, conceptualization; **Thi Kim Hang Pham:** supervision, conceptualization, writing – review & editing.

Conflict of interest

The authors declare that they have no conflict of interest.

References

1. Spencer JA, Mock AL, Jacobs AG, Schubert M, Zhang Y, Tadjer MJ. A review of band structure and material properties of transparent conducting and semiconducting oxides: Ga_2O_3, Al_2O_3, In_2O_3, ZnO, SnO_2, CdO, NiO, CuO, and Sc_2O_3. *Applied Physics Reviews.* 2022;9(1): 011315.

2. Pham TKH, Pham HP, Ngo HDN. Impact of Sputtering Power on Characteristics of Indium-Doped ZnO Thin Films. *Materials Transactions.* 2025;66(9): 1266–1271.

3. Zhang D, Nozaki S, Uchida K. NiO/Si heterostructures formed by UV oxidation of nickel deposited on Si substrates. *Journal of Vacuum Science & Technology B.* 2014;32(3): 031202.

4. Shirshneva-Vaschenko EV, Sosnin IM, Nuryev RK, Gladskikh IA, Liashenko TG, Bezsmertnyĭ VE, Romanov AE. Electrical and optical properties of transparent conducting ZnO:Al/AgNP multilayer films. *Materials Physics and Mechanics.* 2016;29(2): 145–149.

5. Özgür Ü, Alivov YI, Liu C, Teke A, Reshchikov MA, Doğan S, Avrutin V, Cho S-J, Morkoç H. A comprehensive review of ZnO materials and devices. *Journal of Applied Physics.* 2005;98(4): 041301.

6. Egbo KO, Ekuma CE, Liu CP, Yu KM. Efficient p-type doping of sputter-deposited NiO thin films with Li, Ag, and Cu acceptors. *Physical Review Materials.* 2020;4(10): 104603.

7. Sun H, Liao M-H, Chen S-C, Li Z-Y, Lin P-C, Song S-M. Synthesis and characterization of n-type NiO: Al thin films for fabrication of pn NiO homojunctions. *Journal of Physics D: Applied Physics.* 2018;51(10): 105109.

8. Hwang J-D, Lin W-M. Enhancing the photoresponse of p-NiO/n-ZnO heterojunction photodiodes using post ZnO treatment. *IEEE Transactions on Nanotechnology.* 2018;18: 126–131.

9. Tyagi M, Raj VB, Tomar M. High gain NiO/ZnO heterojunction photodiodes operated in Deep-ultraviolet region. *Thin Solid Films.* 2024;798: 140389.

10. Hwang JD, Jiang CI, Hwang SB. P-NiO/n-ZnO heterojunction photodiodes with an MgZnO/ZnO quantum well insertion layer. *Materials Science in Semiconductor Processing.* 2020;105: 104711.

11. Xu Q, Cheng L, Meng L, Wang Z, Bai S, Tian X, Jia X, Qin Y. Flexible self-powered ZnO film UV sensor with a high response. *ACS Appl Mater Interfaces.* 2019;11(29): 26127–26133.

12. Liu KW, Ma JG, Zhang JY, Lu YM, Jiang D, Li B, Zhao DX, Zhang Z, Yao B, Shen DZ. Ultraviolet photoconductive detector with high visible rejection and fast photoresponse based on ZnO thin film. *Solid State Electron.* 2007;51(5): 757–761.

13. Shi Z, Zhang Y, Zhang J, Wang H, Wu B, Cai Xu, Cai Xi, Dong X, Liang H, Zhang B, Du G. High-performance ultraviolet-blue light-emitting diodes based on an n-ZnO nanowall networks/p-GaN heterojunction. *Applied Physics Letters.* 2013;103(2). 021109.

14. Rahman F. Zinc oxide light-emitting diodes: a review. *Optical Engineering.* 2019;58(1): 010901.

15. Rackauskas S, Talka T, Kauppinen EI, Nasibulin AG. Zinc oxide tetrapod synthesis and application for UV sensors. *Materials Physics and Mechanics.* 2012;13(2): 175–180.

16 Khan M, Alam MS, Ahmed SF. Effect of nickel incorporation on structural and optical properties of zinc oxide thin films deposited by RF/DC sputtering technique. *Materials Physics and Mechanics.* 2023;51(1): 19–32.

17. Vyas S. A short review on properties and applications of zinc oxide based thin films and devices: ZnO as a promising material for applications in electronics, optoelectronics, biomedical and sensors. *Johnson Matthey Technology Review.* 2020;64(2): 202–218.

18. Bhosle V, Tiwari A, Narayan J. Electrical properties of transparent and conducting Ga doped ZnO. *Journal of Applied Physics.* 2006;100(3): 033713.

19. Hafdallah A, Ynineb F, Aida MS, Attaf N. In doped ZnO thin films. *Journal of Alloys and Compounds.* 2011;509(26): 7267–7270.

20. Takci DK, Senadim Tuzemen E, Kara K, Yilmaz S, Esen R, Baglayan O. Influence of Al concentration on structural and optical properties of Al-doped ZnO thin films. *Journal of Materials Science: Materials in Electronics.* 2014;25: 2078–2085.

21. Kadam P, Agashe C, Mahamuni S. Al-doped ZnO nanocrystals. *Journal of Applied Physics.* 2008;104(10): 103501.

22. Ohta H, Kamiya M, Kamiya T, Hirano M, Hosono H. UV-detector based on pn-heterojunction diode composed of transparent oxide semiconductors, p-NiO/n-ZnO. *Thin Solid Films.* 2003;445(2): 317–321.
23. Al-Hardan NH, Ahmed NM, Almessiere MA, Aziz AA. Low-intensity UV light sensor based on p-NiO/n-Si heterojunction. *Materials Research Express.* 2020;6(12): 126332.
24. Pham TKH, Tran BQ, Nguyen KB, Pham NYN, Nguyen THY, Nguyen AH-T, Nguyen NP, Ngo HD, Pham HP. Oxygen partial pressure effects on nickel oxide thin films and NiO/Si diode performance. *Materials Advances.* 2025;6(5): 1719–1725.
25. Tsai S-Y, Hon M-H, Lu Y-M. Fabrication of transparent p-NiO/n-ZnO heterojunction devices for ultraviolet photodetectors. *Solid State Electron.* 2011;63(1): 37–41.
26. Gupta RK, Ghosh K, Kahol PK. Fabrication and characterization of NiO/ZnO p–n junctions by pulsed laser deposition. *Physica E: Low-dimensional Systems and Nanostructures.* 2009;41(4): 617–20.
27. San X, Li M, Liu D, Wang G, Shen Y, Meng D, Meng F. A facile one-step hydrothermal synthesis of NiO/ZnO heterojunction microflowers for the enhanced formaldehyde sensing properties. *Journal of Alloys and Compounds.* 2018;739: 260–269.
28. Wei C, Xu J, Shi S, Bu Y, Cao R, Chen J, Xiang J, Zhang X. The improved photoresponse properties of self-powered NiO/ZnO heterojunction arrays UV photodetectors with designed tunable Fermi level of ZnO. *Journal of Colloid and Interface Science.* 2020;577: 279–289.
29. Li C, Feng C, Qu F, Liu J, Zhu L, Lin Y, Wang Y, Li F, Zhou J, Ruan Sh. Electrospun nanofibers of p-type NiO/n-type ZnO heterojunction with different NiO content and its influence on trimethylamine sensing properties. *Sensors and Actuators B: Chemical.* 2015;207: 90–96.
30. Wang T, Liu J, Ma Y, Gu C, Lian J. P-N heterojunction NiO/ZnO electrode with high electrochemical performance for supercapacitor applications. *Electrochimica Acta.* 2021;392: 138976.
31. Tsai SY, Fung KZ. Enhancement of p-NiO/i-ZnO nanorods/n-ZnO ultraviolet detectors through the incorporation of ZnO nanorods. *Journal of Physics and Chemistry of Solids.* 2026;208: 113015.
32. Reddy AM, Reddy AS, Lee K-S, Reddy S. Growth and characterization of NiO thin films prepared by dc reactive magnetron sputtering. *Solid State Sciences.* 2011;13(2): 314–320.
33. Tran BQ, Nguyen KB, Vo NT, Le VT, Do TH, Ngo H, Pham TKH. Effect of limited oxygen gas flux on properties of Al-doped ZnO films. *Dong Thap University Journal of Science.* 2024;13(5): 113–120.
34. Binh NK, Yen Nhi PN, Quan TB, Tam PM, Phuong NN, Tuan DM, Hang PTK, Phuong PH. Impact of in situ heating on the structure, morphology, and electrical and optical properties of RF-sputtered NiO thin films. *Journal of Vacuum Science & Technology B.* 2024;42(6): 062205.
35. Yermakov M, Pshenychnyi R, Opanasyuk A, Klymov O, Mu˜noz-Sanjos´e V. Optical and electrical properties of ZnO/NiO heterojunctions obtained by the spray-pyrolysis method. *Journal of Material Science.* 2024;59: 15738–15751.
36. Chen Z, Dinh HN, Miller E. *UV-vis Spectroscopy. Photoelectrochemical Water Splitting: Standards, Experimental Methods, and Protocols.* New York: Springer; 2013.
37. Ishida Y, Fujimori A, Ohta H, Hirano M, Hosono H. Potential profiling of the nanometer-scale charge-depletion layer in n-ZnO/p-NiO junction using photoemission spectroscopy. *Applied Physics Letters.* 2006;89(15): 153502.
38. Hoai Phuong P, Ngo HD, Bui HT, Phuong NN, Nguyen AHT, Nguyen THY, Tuoi LT, Tran QT, Tuan NM. Effect of sodium doping on characteristics of p-SnOx films prepared by reactive direct current magnetron sputtering. *Ceramics International.* 2022;48(9): 13047–13054.
39. Jlassi M, Sta I, Hajji M, Ben Haoua B, Ezzaouia H. Effect of annealing atmosphere on the electrical properties of nickel oxide/zinc oxide p-n junction grown by sol-gel technique. *Materials Science in Semiconductor Processing.* 2014;26(9): 395–403.
40. Lok R, Dogan MU, Kaya S, Soykan U, Terzioglu C. Gamma radiationinduced modifications in structural, optical, and electrical characteristics of p-NiO/n-Si heterojunction diodes. *Radiation Physics and Chemistry.* 2025;229: 112519.
41. Pham HP, Nguyen THY, Nguyen AH-T, Vo NT, Thuy TGL, Nguyen HH, Hoa HTM, Tran QT. Effects of substrate temperature on characteristics of the p-type Ag-doped SnOx thin films prepared by reactive DC magnetron sputtering. *Journal of Photochemistry and Photobiology A: Chemistry.* 2020;388: 112157.
42. Tyagi M, Tomar M, Gupta V. Trap assisted space charge conduction in p-NiO/n-ZnO heterojunction diode. *Materials Research Bulletin.* 2015;66: 123–131.

43. Gonzalez S, Vescio G, Frieiro JL, Hauser A, Linardi F, Lopez-Vidrier J, Oszajca M, Hernandez S, Ciera A, Garrido B. Inkjet-Printed p-NiO/nZnO Heterojunction Diodes for Photodetection Applications. *Advanced Materials Interfaces.* 2023;10(15): 2300035.
44. Huang J, Li B, Hu Y, Zhou X, Zhang Z, Ma Y, Tang K, Wang L, Lu Y. Transparent p-NiO/n-ZnO heterojunction ultraviolet photodetectors prepared on flexible substrates. *Surface and Coatings Technology.* 2019;362: 57–61.
45. Lin X-Y, Chang H-C, Huang B-L, Lin Y-J. Induced transition from Schottky to ohmic contact in In/n-type Si owing to $(NH_4)_2S_x$ treatment. *Indian Journal of Physics.* 2022;96: 3137–3141.
46. Hakkoum H, Moumen A, Ghougali M, Sengouga N, Comini E. The effect of structural characteristics of ZnO and NiO thin films on the performance of NiO/ZnO photodetectors. *Journal of Materials Science: Materials in Electronics.* 2022;33: 26604–26618.
47. Deng R, Yao B, Li YF, Zhao YM, Li BH, Shan CX, Zhang ZZ, Zhao DX, Zhang JY, Shen DZ, Fan XW. X-ray photoelectron spectroscopy measurement of n-ZnO/p-NiO heterostructure valence-band offset. *Applied Physics Letters.* 2009;94(2): 022108.
48. Grundmann M, Karsthof R, von Wenckstern H. Interface recombination current in type II heterostructure bipolar diodes. *ACS Applied Materials & Interfaces.* 2014;6(17): 14785–14789.